

# Impact of Different Conditions of Technological Process on Thermoelectric Properties of Fine-Grained PbTe

A. KRÓLICKA\*, A. MATERNA, M. PIERSA AND A. MIROWSKA

Institute of Electronic Materials Technology, Wólczyńska 133, 01-919 Warsaw, Poland

The aim of this work was to obtain PbTe material in the desired way in order to control the combined impact of lattice disorder, nanoscale precipitates and reduced grain sizes on the thermoelectric properties of this material. To achieve this, PbTe ingot doped with Ag was obtained by the Bridgman method, followed by ball-milling, cold pressing and sintering. In order to estimate crystallites diameters grain size measurements were carried out using the optical microscopy. Studies of electrical and thermoelectric properties of fine-grained material were performed. In order to analyze the morphology and the composition scanning electron microscopy and energy-dispersive X-ray spectroscopy were performed. Energy-dispersive X-ray spectroscopy analysis also revealed presence of Ag-Te precipitates.

DOI: [10.12693/APhysPolA.130.1255](https://doi.org/10.12693/APhysPolA.130.1255)

PACS/topics: 81.10.Fq, 73.20.Hb, 81.20.Wk, 81.20.Ev

## 1. Introduction

The efficiency of thermoelectric materials is determined by the following parameters: thermal conductivity, electrical conductivity, and the Seebeck coefficient, giving the figure of merit ( $ZT$ ) of the thermoelectric material. This is given by the following formula:

$$ZT = \frac{S^2 \sigma}{\kappa} T, \quad (1)$$

where  $\sigma$  is the electrical conductivity,  $S$  is the Seebeck coefficient and  $\kappa$  is the thermal conductivity. The values  $S$ ,  $\kappa$  and  $\sigma$  are in fact closely related with each other and finding a compromise between them is a very difficult and important issue.

According to the literature [1], conducting the technological processes in the controlled and optimal way can be realized by multi-scale structure modification. As was reported, approximately 80% of thermal conductivity ( $\kappa_l$ ) in PbTe:Na doped with Sr is due to phonon-modes with mean free path lengths less than 100 nm. Such phonon modes can be suppressed by combination of the control of crystal structure and selecting the appropriate compositional elements in the atomic scale (e.g. via doping with La, Cr), nanoscale precipitates (exemplary by adding Ag [2–4]) and by incorporating stresses and dislocations (for example by quenching in cold water). The remaining 20% of  $\kappa_l$  in PbTe is caused by phonon modes with a mean free path length ranging from 0.1  $\mu\text{m}$  to 1 mm. These modes can be scattered on the grain boundaries in mesoscale, either by milling the material in an appropriate way and the structure obtained by spark plasma sintering. Using all of these approaches at the same time (scattering of phonons in atomic scale, nanometer scale and mesoscale) gives opportunity for achieving high thermoelectric performance in PbTe.

In order to obtain high  $ZT$ , it is necessary to fabricate materials with appropriate value of  $n/p$  carrier concentration. As was previously reported [5, 6], the optimal free carrier concentration should be in the range of  $10^{19} - 10^{21} \text{ cm}^{-3}$  and this is realized through appropriate doping. Information about various dopants effect on electrical properties of PbTe can be found elsewhere [7–11].

The way in which Ag atoms occupy crystal sites in PbTe can be explained by taking into consideration the temperature dependent solubility of silver in PbTe [12, 13]. This also explains distinctive electrical-transport properties of various PbTe(Ag) systems. At low temperature, silver solubility in PbTe is very low, hence the Ag atoms, acting as acceptors occupy the Pb sites. This leads to the decreased carrier concentration and enhanced carrier mobility. As the temperature increases, the solubility of Ag rises. The Ag atoms occupy the interstitial sites and act as donors. This contributes to the carrier concentration increase [12–14].

Recently, Capelli et al. [15] demonstrated results for PbTe(Ag) alloys with atomic percentage Ag content (1–20%). Increasing the Ag content up to 5 at.% resulted in the  $p$ -type conductivity with carrier concentration value of  $\approx 10^{19} \text{ cm}^{-3}$ . After exceeding this content conduction behavior changed and system turned out to be an  $n$ -type semiconductor. However, the highest power factor value of  $3.36 \mu\text{W K}^{-2} \text{ cm}^{-1}$  was obtained for 5 at.% Ag content. Also high thermoelectric values for PbTe doped with similar Ag content (5.3 at.% Ag) were obtained by Pei and co-workers [2]. They fabricated the nanograined material with Ag precipitates distributed homogeneously in the matrix and for the mentioned Ag content, highest Seebeck coefficient of  $\approx 300 \mu\text{V/K}$  ( $T = 500 \text{ K}$ ) and the lowest thermal conductivity of  $\approx 1 \text{ W/mK}$  (due to phonon scattering on Ag-Te inclusions) were obtained.

Silver is readily used in order to improve the electrical properties of PbTe compounds by many research groups, for example Zhang et al. fabricated  $(\text{PbTe}_{0.9}\text{S}_{0.1})_{1-x}(\text{Ag}_2\text{Te})_x$  alloys with small amounts of

\*corresponding author; e-mail: [aleksandra.krolicka@itme.edu.pl](mailto:aleksandra.krolicka@itme.edu.pl)

Ag ( $x = 0, 0.01, \text{ and } 0.03$ ) [16]. The increase in the carrier concentration, as compared with the  $\text{Ag}_2\text{Te}$ -free sample, was observed above 473 K. This resulted in high power factor of  $0.11 \text{ W K}^{-2} \text{ cm}^{-1}$  at 573 K for the sample with  $x = 0.03$ . Additionally, the thermal conductivity decrease was obtained. Such a behavior was also reported for similar systems:  $\text{Ag}_2\text{Te}$ -doped PbTe and Ag-doped PbTe/ $\text{Ag}_2\text{Te}$  samples [2, 17].

In the present paper, we discuss the effect of Ag doping and Ag inclusions on the electrical and thermoelectric properties of the ball-milled, cold-pressed, and sintered PbTe. We compare the obtained results with the undoped as-grown material.

## 2. Experimental

In the present study vertical Bridgman technique was used to obtain polycrystalline  $(\text{PbTe})_{1-x}(\text{Ag}_2\text{Te})_x$  material, where  $x = 5.5 \text{ at.}\%$ . Conditions of synthesis and crystallization processes were selected according to the literature [2]. Appropriate amounts of pure elements were loaded into a quartz ampoule, followed by sealing under vacuum of  $\approx 10^{-6} \text{ Torr}$ . Material was heated up to  $1000^\circ\text{C}$  and soaked at this temperature for 6 h. Subsequently, the ampoule was cold-water quenched. This was followed by the first annealing at  $700^\circ\text{C}$  for two days for homogenization and cold-water quenching again. This resulted in formation of strains and stresses in the material, which was the intended effect. Figure 1 shows a crack running along the crystal, revealing its fragile structure.

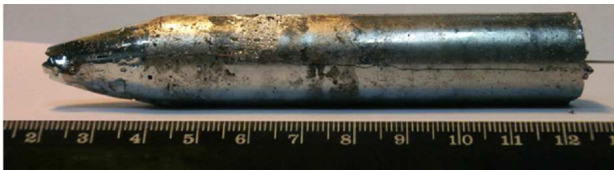


Fig. 1. Polycrystalline ingot of PbTe doped with silver.

In order to obtain Ag-Te precipitates the ampoule was re-annealed, second annealing was conducted at  $500^\circ\text{C}$  for three days. This can be explained as follows: silver has the highest solubility in PbTe at  $700^\circ\text{C}$  (7–11 mol.%) and its solubility limit decreases with decreasing temperature, reaching a value of 1 mol.% at  $T = 500^\circ\text{C}$ . Thus,  $\text{Ag}_2\text{Te}$  precipitates will emerge most effectively during annealing at lower temperature. This has already been demonstrated by at least a few scientific groups [2, 14, 18, 19] and is consistent with the current study.

Sintered cylindrical pellets were produced following the procedure of ball-milling of the obtained ingot, cold-pressing and sintering (we will use the name CPS) in a horizontal programmable tube furnace. Fragmentation was conducted in the high-energy ball mill for 1 h. Milling-jar and balls were made up of stainless steel. Material was cold-pressed under a pressure of 3 MPa.

Sintering temperature and time were  $600^\circ\text{C}$  and 3 h, respectively.

Here, we present results of the thermoelectric measurements of the undoped as-grown PbTe in comparison with the fine-grained material. The crystal structure and chemical composition of the obtained sintered pellets were analyzed using scanning electron microscopy (SEM) and energy-dispersive X-ray spectroscopy (EDX). The measurements of grain diameters were carried out.

## 3. Results and discussion

### 3.1. Grain size measurements

To determine the grain size of obtained powders, studies of the particle diameters were performed using the optical microscopy (image analysis system — Clemex vision). Based on this analysis, the smallest particle diameters were 200 nm, and 78.12% were particles with diameters ranging from 200 to 300 nm (Fig. 2a,b). However, it should be noticed that PbTe has a strong tendency to agglomerate, hence presence of agglomerates should be taken into account when analyzing the results. Nevertheless, it has been indicated that fine-grained powders can be obtained in a fairly low time line.

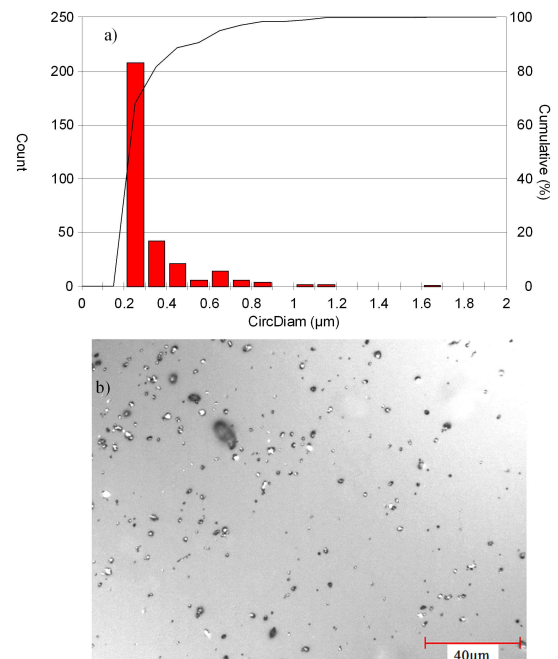


Fig. 2. Grain size measurements of the PbTe(Ag) powder: (a) bar diagram of the analyzed powder; particles diameters were found to be in the range of 0.2–1.7  $\mu\text{m}$  and the mean value was 0.4  $\mu\text{m}$ , (b) image taken through an optical microscope, displaying powder particles and agglomerates of particles. Image scale is 40  $\mu\text{m}$ .

### 3.2. SEM and EDX analysis

Figure 3 shows SEM image of the sintered pellets. As can be seen, material is composed of layers, irregular in shape and size, embedded one on another, perhaps this is a lamellar structure, which has been mentioned in the literature of PbTe doped with silver [2, 6].

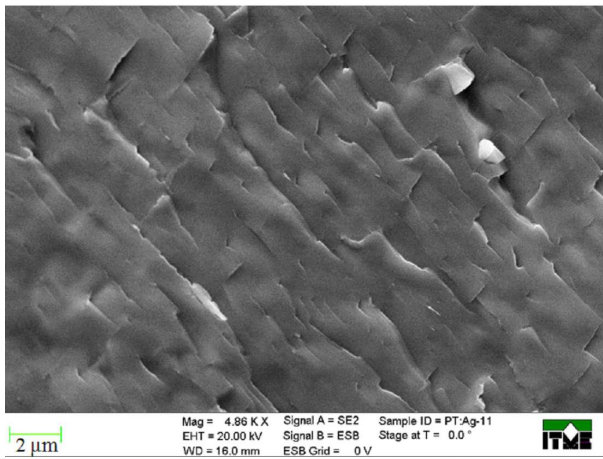


Fig. 3. SEM image of the CPS pellet.

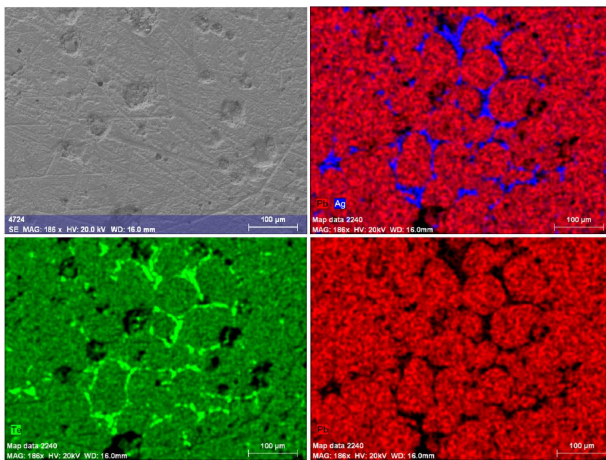


Fig. 4. SEM images of CPS PbTe(Ag) obtained by EDS microanalysis, indicating the formation of secondary phases containing both — silver and tellurium SEM image of CPS PbTe(Ag) sample and EDS microanalysis results, indicating the formation of secondary phases containing both — silver and tellurium.

Figure 4 shows energy dispersive spectroscopy (EDS) maps for the PbTe(Ag) sintered pellets. The maps indicate that Pb atoms are displaced by the Ag and Te atoms resulting in formation of secondary phases, which prefer to locate in the pores (material was not optimally densified, the applied pressing pressure was 3 MPa). Such

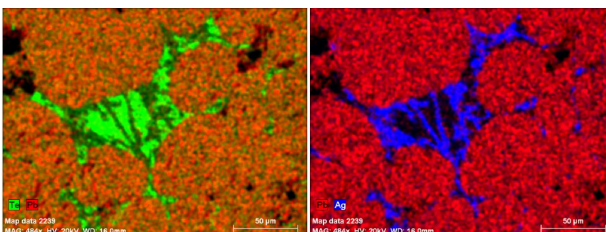


Fig. 5. SEM images of CPS PbTe(Ag) obtained by EDS microanalysis, indicating the formation of single Ag- and Te-inclusions (both elements are located close to each other but they do not occupy the same places).

results of the EDS analysis may also be connected with the lamellar structure, mentioned above. As can be seen in Fig. 5, secondary phases containing Ag and Te are present in the form of single Ag- and Te-inclusions as well as containing both elements, probably as  $\text{Ag}_2\text{Te}$  [2]. Thus obtained inclusions result in the phonon scattering enhancement, which contributes to thermal conductivity decrease.

### 3.3. Electrical and thermoelectric measurements

Electrical resistivity and the Hall measurements for the as-grown and CPS samples were carried out by the Van der Pauw technique. The Seebeck coefficient was measured using set of two heaters — one acting as a heat source and second, as a heat sink. The Seebeck coefficient was determined from the ratio of the measured thermoelectric power and the temperature difference. The thermal conductivity was determined from the following formula:

$$\kappa(T) = \rho(T) C_p(T) \alpha(T), \quad (2)$$

where  $\rho$  — density,  $C_p$  — the specific heat (measured using the simultaneous thermal analysis — NETZSCH STA 449F1) and  $\alpha$  — the thermal diffusivity (measured using the laser flash method — laser flash apparatus LFA 457).

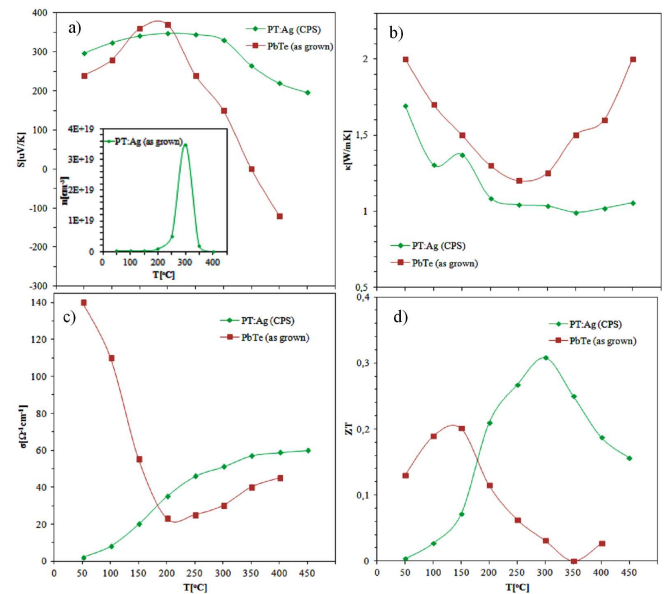


Fig. 6. (a) Seebeck coefficient and electron concentration (inset) of the as-grown PbTe(Ag), (b) thermal conductivity, (c) electrical conductivity and (d) figure of merit versus temperature; comparison of the undoped as-grown PbTe (red line) and CPS PbTe(Ag) (green line).

Figure 6 shows the temperature dependences of the thermoelectric parameters for the undoped as-grown PbTe and CPS PbTe(Ag) material. As revealed in Fig. 6a, very high values of the  $p$ -type Seebeck coefficient were obtained for both samples. After reaching

the highest value of 347  $\mu\text{V}/\text{deg}$  at 200 °C, the Seebeck coefficient of CPS begins to decrease rapidly, which can be attributed to the bipolar contribution to conductivity [20]. This is consistent with the obtained carrier concentration results for this sample (see the inset in Fig. 6a). Also the thermal conductivity (Fig. 6b) exhibits intrinsic semiconducting behavior and at high temperatures the bipolar contribution becomes significant. The reduction in  $\kappa$  was obtained as compared to the as-grown PbTe. The lowest values of  $\kappa$  for the undoped PbTe and CPS PbTe were 1.2 at 250 °C and 0.99 at 350 °C, respectively. However, the obtained values for CPS sample are not very low, which is explained by the micrometer sized grains (instead of nanometer) obtained during ball-milling (the majority of grains diameters ranged from 200 to 300 nm). The increase in electrical conductivity with temperature for CPS sample (Fig. 6c) clearly shows the behavior of a non-degenerate semiconductor and contributes to the maximal  $ZT$  value, which is 0.3 at 300 K (Fig. 6d). These findings are consistent with the obtained carrier concentration results. The results show that the highest carrier concentration temperature overlap with the highest  $ZT$  temperature. This confirms a strong impact of carrier concentration on the performance of thermoelectric materials.

#### 4. Summary and conclusions

The investigation indicated that the multiscale structure modification can result in significant improvement of the thermoelectric properties of silver doped PbTe. Due to annealing and cold-water-quenching strains and lattice distortions were obtained. Additionally, annealing resulted in generating Ag-, Te-, and Ag-Te precipitates. The mentioned activities including the eventual ball-milling resulted in obtaining majority of grains with diameters ranging from 200 to 300 nm and effective scattering of mid- and long-wavelength phonons was realized. Hence, reduction of thermal conductivity as compared to the as-grown PbTe was obtained. The ball-milling procedure also resulted in the Seebeck coefficient enhancement. Finally, the  $ZT$  value of 0.3 was obtained at 300 °C.

#### References

- [1] K. Biswas, J. He, I.D. Blum, C.I. Wu, T.P. Hogan, D.N. Seidman, V.P. Dravid, M.G. Kanatzidis, *Nature* **489**, 414 (2003).
- [2] Y. Pei, J. Lensch-Falk, E.S. Toberer, D.L. Medlin, G. Jeffrey Snyder, *Adv. Funct. Mater.* **21**, 241 (2011).
- [3] T. Ikeda, S. Iwanaga, H. Wu, N.J. Marolf, S. Chenc, G.J. Snyder, *J. Mater. Chem.* **22**, 24335 (2012).
- [4] Y. Pei, A.F. May, G.J. Snyder, *Adv. En. Mater.* **1**, 291 (2011).
- [5] P. Vaquero, A.V. Powell, *J. Mater. Chem.* **20**, 9577 (2010).
- [6] H. Wu, W. Foo, S. Chen, G.J. Snyder, *Appl. Phys. Lett.* **101**, 023107 (2012).
- [7] Z.H. Dughaish, *Physica B* **322**, 205 (2002).
- [8] Y. Gelbstein, Z. Dashevsky, M.P. Dariel, *Physica B* **363**, 196 (2005).
- [9] J.P. Heremans, B. Wiendlocha, A.M. Chamoire, *En. Environm. Sci.* **5**, 5510 (2012).
- [10] Y. Takagiwa, Y. Pei, G. Pomrehn, G.J. Snyder, *Appl. Phys. Lett.* **101**, 092102 (2012).
- [11] Ch. Papageorgiou, J. Giapintzakis, Th. Kyratsi, *AIP Conf. Proc.* **1449**, 135 (2012).
- [12] Y. Noda, M. Orihashi, I.A. Nishida, *Mater. Trans. JIM* **39**, 602 (1998).
- [13] M. Orihashi, Y. Noda, H.T. Kaibe, I.A. Nishida, *Mater. Trans. JIM* **39**, 672 (1998).
- [14] F.J. Wald, *J. Less-Comm. Met.* **13**, 579 (1967).
- [15] E. Cappelli, A. Bellucci, L. Medici, A. Mezzi, S. Kaciulis, F. Fumagalli, F. Di Fonzo, D.M. Trucchi, *Appl. Surf. Sci.* **336**, 283 (2015).
- [16] H. Zhang, J. Luo, H. Zhu, J. Liang, L. Ruan, Q. Liu, J. Li, G. Liu, *Acta Mater.* **60**, 7241 (2012).
- [17] K. Ahn, Ch. Li, C. Uher, M.G. Kanatzidis, *Chem. Mater.* **21**, 1361 (2009).
- [18] *ASM Alloy Phase Diagrams Center.*
- [19] R. Blachnik, B. Gather, *J. Less-Comm. Met.* **60**, 25 (1978).
- [20] J.J. Martin, G.C. Danielson, *Phys. Rev.* **166**, 879 (1968).